


Numerical Investigation of Thermal and Mechanical Responses in PEMFC Under Combined Loading Conditions

Safiye Nur Özdemir 

Sakarya University, Engineering Faculty, Department of Mechanical Engineering, Sakarya, Türkiye, safiyeozdemir@sakarya.edu.tr, ror.org/04ttnw109

ARTICLE INFO

ABSTRACT

Keywords:
PEM fuel cell
Temperature distribution
Thermal stress
Thermo-mechanical stress
Numerical simulation



Article History:
Received: 24.08.2025
Revised: 06.11.2025
Accepted: 08.12.2025
Online Available: 30.01.2026

The mechanical and thermal responses of Proton Exchange Membrane Fuel Cells (PEMFCs) under various temperature loadings and clamping forces are essential for their operational performance and reliability. In this investigation, the thermo-mechanical performance of the PEMFC was examined under clamping force and varying temperature loads using numerical simulations conducted with ANSYS software. Focusing on the thermal stresses generated in the membrane, often considered the core component of the PEMFC, under different temperature conditions, along with the corresponding temperature distributions within the cell. Thermo-mechanical analyses were conducted with a fixed clamping torque of 10 Nm. The thermal stress analysis indicated that the maximum stress on the membrane nearly doubled when the operating temperature increased from 50 °C (1.006 MPa) to 80 °C (2.083 MPa). This increase was primarily attributed to the mismatch in thermal expansion coefficients between adjacent layers. Moreover, under a 10 Nm clamping torque, the combined thermo-mechanical stress decreased gradually by about 9% with increasing temperature, indicating that the applied mechanical compression compensates the thermally induced stresses. These findings reveal that the applied clamping torque not only governs the stress distribution but also compensates for thermally induced deformations, thereby enhancing the structural stability and durability of the membrane. The results provide valuable engineering insight for improving the thermo-mechanical reliability and long-term performance of PEMFC assemblies.

1. Introduction

As global energy demand rises, hydrogen-based technologies can reduce reliance on fossil fuels and help mitigate environmental issues. Hydrogen fuel cell technology is a promising alternative for decarbonizing the transportation sector, especially compared to traditional fossil fuel-based technologies. In recent years, fuel cell technology has gained popularity in vehicles. These fuel cells can operate under various conditions; buses and trains typically have stable load profiles, while passenger cars and delivery vehicles often experience fluctuating loads [1-3]. Hydrogen fuel cells are categorized based on the electrolyte material used, including proton exchange membrane fuel cells (PEMFCs), solid

oxide fuel cells (SOFCs), phosphoric acid fuel cells (PAFCs), molten carbonate fuel cells (MCFCs), and alkaline fuel cells (AFCs) [4]. PEMFCs are a promising energy conversion technology that utilizes hydrogen as fuel, providing a viable path towards clean and sustainable energy systems. PEMFCs offer high efficiency and environmentally friendly operation, generating electricity without producing harmful emissions [5].

A typical PEMFC comprises several key components, including end plates, current collector (CC) plates, bipolar plates (BPs), porous transport layers (PTLs), and a membrane electrode assembly (MEA). The MEA is the core component of a PEMFC, consisting of a proton

exchange membrane placed between catalyst layers on both the anode and cathode sides. The durability of the MEA is essential for the overall lifespan of a PEMFC [6]. However, over time, the performance of the MEA can decline due to factors such as material properties, manufacturing processes, and operational conditions. Degradation of fuel cell components over time typically falls into three main categories: mechanical, chemical, and thermal [7]. These degradations reduce cell performance and negatively affect the long-term reliability of the system.

Mechanical stresses result from the compression forces applied during the assembly process of PEMFCs. In contrast, thermal stresses arise during production and operational conditions due to the varying thermal expansion coefficients of the fuel cell components. Therefore, a detailed understanding of the various mechanisms that cause stress generation and their effects on cell performance is critical for the long-term durability and service life of PEMFC systems [8]. Numerous numerical modeling studies and experimental analyses have been conducted in the literature to reveal the mechanical and thermal response characteristics of PEMFC systems.

Jiang et al. [9] conducted both experimental and numerical analyses on single-cell and 40-cell PEMFC to identify the optimal compression pressure for maximizing power output and achieving a more uniform contact pressure distribution. They found this optimal compression pressure to be approximately 1.33 MPa.

Ozdemir and Kurt [10] conducted a thorough finite element analysis on a PEMFC stack, incorporating an innovative hydraulic assembly system that differs from the traditional screw assembly mechanism. They aimed to understand how the PEMFC stack assembly method affects the mechanical stresses and deformations experienced by the components. The numerical analysis results indicate that the new compression mechanism reduces the von Mises stresses on the membrane by approximately 12.9% compared to the conventional design.

Yilgin et al. [11] conducted an experimental investigation on the effects of three design parameters—tightening torque, bolt configuration, and end plate material—on the compression ratio of the pressure-sensitive film used in place of the MEA. The optimal design conditions were achieved by utilizing a stainless steel end plate and applying a mounting torque of 9 Nm. Additionally, the assembly consisted of a total of 8 bolts. Under these conditions, the compression ratio measured on the pressure film was determined to be 63.51%.

Jing et al. [12] comprehensively investigated the effects of clamping torque on structural deformations and contact resistance in PEMFC components, assessing the role of these parameters on both cell durability and electrochemical performance. They achieved that when an optimum compression force is applied, a 2.77% improvement in current density is observed at a cell voltage of 0.45 V, compared to the case without compression.

Oh et al. [13] developed a three-dimensional FE model for a high-temperature PEMFC (HT-PEMFC) and analyzed the thermal stresses induced by the operating temperature in the cell components. The numerical analysis results indicate that significant thermal stresses arise with increasing temperature, particularly in the membrane and catalyst layers that comprise the MEA.

In their work, Bates et al. [14] utilized ANSYS Mechanical to simulate the mechanical behavior of a 100 cm² active area PEMFC under a range of clamping pressure conditions. Among all structural components, the end plates of the 16-cell PEM fuel cell stack were subjected to the highest mechanical loading, reaching a peak stress of 183.1 MPa.

Al-Baghdadi [15] established a 3D multiphysics simulation model of a PEMFC and investigated its thermal behavior by accounting for variations in temperature and relative humidity. The results indicated that thermal stress gradients arising from non-uniform temperature distribution cause localized flexural stresses, elevating the potential for crack initiation in the cell.

Sun et al. [16] examined the effect of clamping force on GDL deformation, thermal contact resistance (TCR), and electrical contact resistance (ECR). They concluded that the optimal installation pressure for the PEMFC is 1 MPa, and noted that increases in assembly pressure adversely impact the uniformity of temperature distribution within the cell components.

Chippar et al. [17] conducted an extensive numerical study to investigate how the deformation of the PTL affects the performance of an HT-PEMFC. They integrated an FEM with a computational fluid dynamics (CFD) model in their analysis. The results showed that increasing the PTL compression ratio resulted in significant spatial variations in hydrogen and oxygen concentrations and in the distribution of current density. Notably, at a 25% displacement, the maximum mechanical stress in the PTL reached 4.11 MPa, surpassing the structural strength threshold and indicating a risk of irreversible structural damage.

Zhang et al. [18] studied a PEMFC structure that used steel straps instead of the conventional screw mechanism. They conducted a numerical analysis to evaluate how variations in the number of straps, strap widths, and assembly forces affected the stress distribution and contact pressure within the fuel cell components. When

a force of 25 kN was applied, the average contact pressure reached its maximum value.

The objective of this study is to establish a three-dimensional simulation tool for PEMFCs that couples structural and thermal domains, enabling a comprehensive evaluation of the cell's response to a range of operating temperatures. Most studies have focused on the stresses and deformations caused by the clamping torque applied during PEMFC assembly. In contrast, this study also considers the effects of temperature-induced variations, aiming to capture the combined thermo-mechanical behavior of the cell components. This integrated approach provides a more accurate assessment of the stresses experienced by the membrane under actual operating conditions.

2. Numerical Methodology

The three-dimensional simulation model was constructed using ANSYS SpaceClaim software. The overall computational domain of a PEMFC and its main functional components are illustrated in Figure 1. Table 1 summarizes the geometric dimensions of the PEMFC components employed in the numerical model. The material and thermal properties of the individual PEMFC components are presented in Table 2.

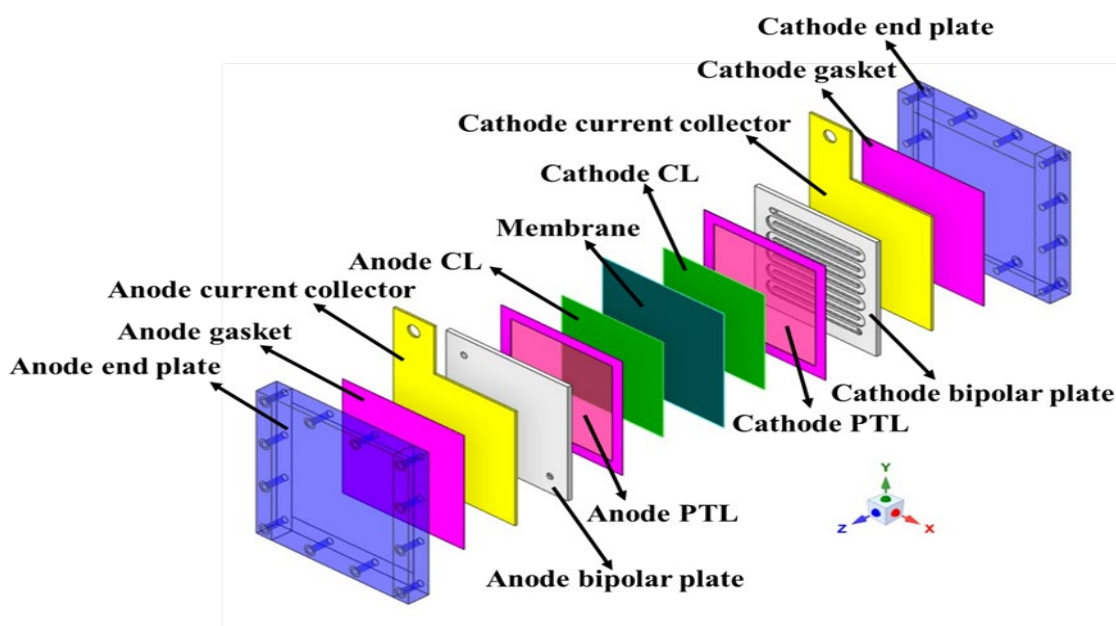


Figure 1. Three-dimensional exploded view of the components of a PEMFC simulation model

Table 1. Geometric parameters for numerical simulation

Components	Dimensions (mm)	Thickness (mm)
End plate	150 × 150	20
Gasket	120 × 120	0.26
Current collector	120 × 120	2
Bipolar plate	120 × 120	4
PTL	100 × 100	0.26
CL	100 × 100	0.015
PEM	120 × 120	0.125

Table 2. Thermo-mechanical properties of the PEMFC components [19]

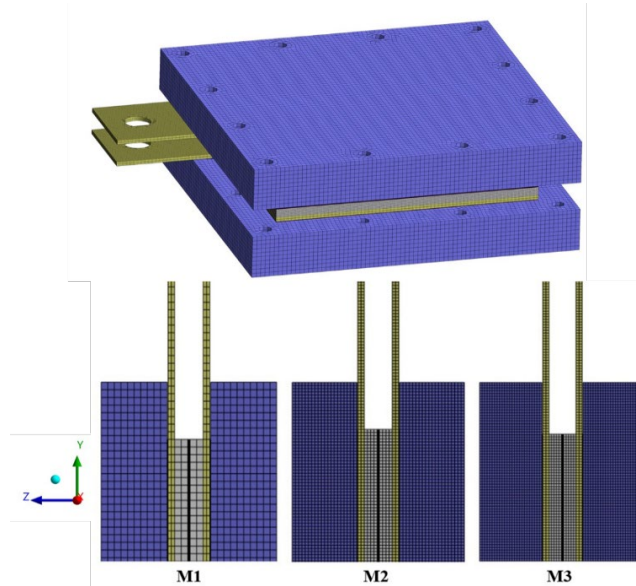
Components	Material	Elasticity modulus (GPa)	Poisson ratio (-)	Thermal conductivity (W/mK)	Coefficient of thermal expansion (K ⁻¹)
End plate	Stainless steel	209	0.25	44.5	12 · 10 ⁻⁶
Gasket	Silicon	0.54	0.30	0.517	62 · 10 ⁻⁶
Current collector	Copper	110	0.35	385	17 · 10 ⁻⁶
Bipolar plate	Graphite	10	0.25	95	5 · 10 ⁻⁶
PTL	Carbon paper	10	0.25	17.122	0.8 · 10 ⁻⁶
MEA	Nafion	0.021	0.25	0.455	123 · 10 ⁻⁶

As shown in Figure 2, the computational mesh of the PEMFC is shown for both the full assembly and the cross-sectional view. To ensure the accuracy of the solutions, a mesh independence study was conducted using three different mesh densities, as detailed in Table 3. The tested mesh configurations consisted of 220407 elements (M1), 1138468 elements (M2), and 2409561 elements (M3) (see Figure 2). The average temperature-induced stress on the membrane showed minimal variation between the M2 and M3 meshes, with a relative error of only 0.01%. Based on these findings, the M2 mesh was sufficiently accurate, providing an optimal balance between computational load and numerical precision. The assembly conditions were established at a reference temperature of 22 °C, where the thermal stresses of all cell components were assumed to be zero. During the assembly process, clamping torques generated by the bolts and nuts were applied to specific areas of the end plates, and the cell was secured using twelve bolts. The proposed model also considers factors such as bolt diameter and friction coefficients involved in the assembly process. A clamping torque of 10 Nm was applied with a friction coefficient of 0.2. Additionally, no heat

generation was considered under the specified boundary conditions. The bolts were arranged in a cross-pattern to ensure uniform compression across the cell assembly. This configuration reduces local stress concentrations and promotes mechanical symmetry. A total of twelve bolts were evenly positioned on the end plates, and a clamping torque of 10 Nm was applied, in line with standard configurations reported in previous experimental and numerical studies on PEMFCs. A friction coefficient of 0.2 was used to represent the contact interaction between the bolts and the end plates, consistent with standard mechanical assembly practices. Furthermore, a constant temperature condition was assumed since no internal heat generation was considered within the computational domain. The main goal was to assess the thermo-mechanical response based on specified operating temperatures and clamping torque. The temperature boundary conditions applied in the model inherently reflect the overall thermal field that develops during operation. The inlet temperatures of the reactants were varied within the range of 50 to 80 °C to evaluate their effects on the thermo-mechanical behavior of the membrane

Table 3. Mesh independence test

Mesh Number	Number of elements	Number of nodes	Temperature-induced average stress on the membrane (MPa)	Relative error (%)
M1	220407	253477	0.46667	-
M2	1138468	1157213	0.46733	0.14143
M3	2409561	2693603	0.46738	0.01070

**Figure 2.** Finite element mesh of the PEMFC: full assembly and different mesh numbers

The governing equation for heat transfer can be expressed as [20],

$$\nabla \cdot (\lambda^{eff} \nabla T) = 0 \quad (1)$$

Where T denotes the temperature and λ^{eff} indicates the effective thermal conductivity. In this study, the elastic deformation of the PEMFC can be attributed to the applied clamping force and the temperature gradient. The strain induced by the temperature gradient can be expressed as follows:

$$\varepsilon^T = \alpha \Delta T \quad (2)$$

Where ΔT is the temperature difference, ε^T is the thermal strain, and α is the coefficient of thermal expansion. Therefore, the strain resulting from combined loadings can be described as follows [21]:

$$\varepsilon_x = \frac{1}{E} [\sigma_x - \mu(\sigma_y + \sigma_z) + \alpha \Delta T] \quad (3a)$$

$$\varepsilon_y = \frac{1}{E} [\sigma_y - \mu(\sigma_z + \sigma_x) + \alpha \Delta T] \quad (3b)$$

$$\varepsilon_z = \frac{1}{E} [\sigma_z - \mu(\sigma_x + \sigma_y) + \alpha \Delta T] \quad (3c)$$

Where E is the elastic modulus, μ is Poisson's ratio, σ is the normal stress, and ε is the normal strain. The equivalent (von Mises) stress can be defined by [22],

$$\sigma_e = \sqrt{\frac{1}{2} [(\sigma_x - \sigma_y)^2 + (\sigma_y - \sigma_z)^2 + (\sigma_z - \sigma_x)^2 + 6(\tau_{xy}^2 + \tau_{yz}^2 + \tau_{zx}^2)]} \quad (4)$$

3. Results and Discussion

The membrane is one of the most sensitive components of the PEMFC and can deform when exposed to assembly loads caused by uneven pressure distributions. Damage from mechanical and thermal stresses is often more critical than electrochemical degradation and can lead to sudden failure. It is crucial to apply the appropriate clamping torque to optimize energy efficiency and prevent gas leakage in the PEMFC. Excessive clamping torque can crush the membrane, while insufficient torque may lead to poor contact between components and increase the risk of gas leakage.

In practice, the optimum clamping torque has been reported to be 10 Nm. For the purposes of this study, this clamping force was treated as a constant value, and numerical analyses based on FEM were conducted accordingly. This study performed numerical calculations using solid mechanics and thermal analysis to assess thermal and mechanical stresses in a PEMFC at different operating temperatures and under a clamping torque of 10 Nm. The cell consists of 12 bolts with a 6 mm bolt hole diameter.

Before interpreting the numerical results, it is crucial to highlight that thermal stresses generated within PEMFC components due to temperature variations, along with mechanical stresses induced by the applied clamping force during assembly, significantly impact the electrochemical performance, durability, and overall service life of the cell. The number of studies examining these coupled thermo-mechanical effects, particularly in the context of PEMFCs, is still relatively limited in the existing literature. Therefore, this study aims to fill that gap by providing a systematic investigation that can serve as a valuable reference for fuel cell manufacturers, researchers, and students involved in the field of hydrogen technologies.

Figure 3 shows the temperature distribution in the PEMFC simulation model for different

reactant inlet temperatures. At an inlet temperature of 50 °C, the maximum temperature recorded was 50.326 °C, while the minimum temperature was 42.38 °C. When the inlet temperature increased to 60 °C, the maximum temperature rose to 60.442 °C, and the minimum temperature was 49.659 °C. For an inlet temperature of 70 °C, the maximum and minimum temperatures recorded were 70.6 °C and 56.937 °C, respectively. Under the highest operating condition of 80 °C, the maximum temperature reached 80.7 °C, with a corresponding minimum value of 64.216 °C. The temperature distribution within a PEMFC significantly influences both the kinetics of the electrochemical reactions and the water content of the membrane.

While higher temperatures can enhance ionic conductivity and improve reaction rates, excessive thermal gradients may result in membrane dehydration and localized thermal stresses [23]. Simulation results indicate that increasing temperatures heighten the risk of forming local hot spots. These hot spots are mainly observed in the membrane electrode assembly (MEA), particularly in the central region, as illustrated in the side views. Such conditions can accelerate material degradation during prolonged operation and ultimately shorten the lifespan of the PEMFC.

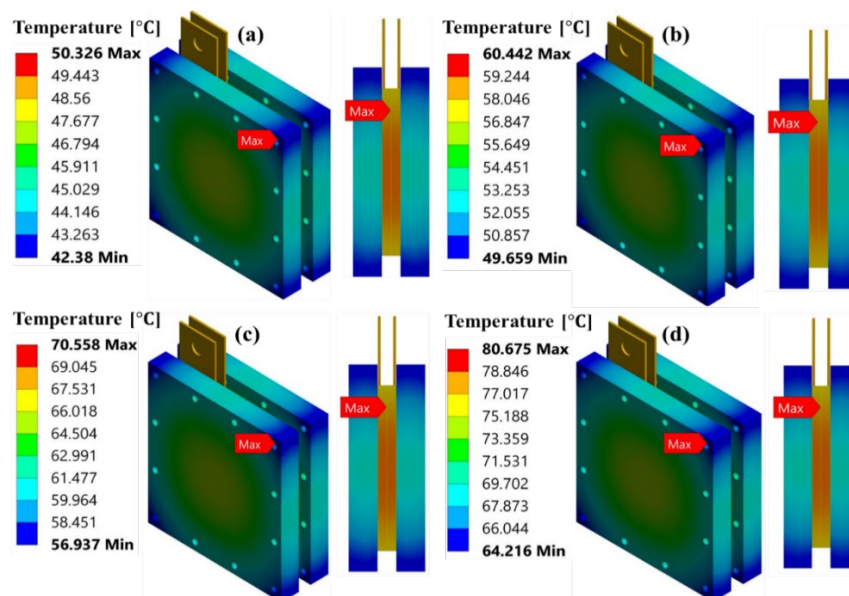


Figure 3. Comparison of PEMFC temperature distributions for reactant inlet temperatures of 50 °C (a), 60 °C (b), 70 °C (c), and 80 °C (d)

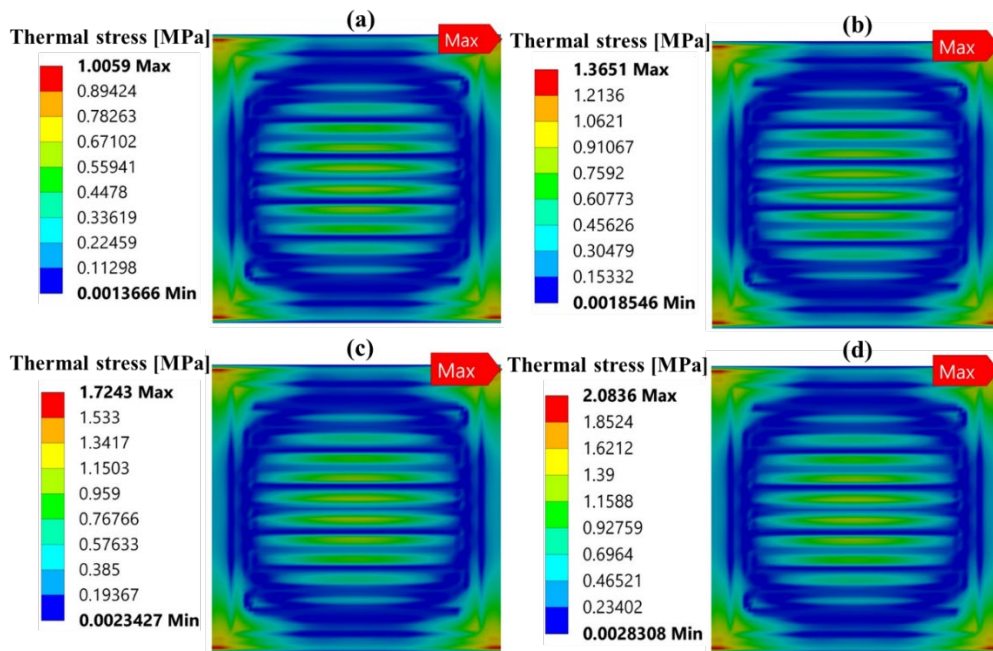


Figure 4. Thermal stress distributions (MPa) on the membrane at operating temperatures of 50 °C (a), 60 °C (b), 70 °C (c), and 80 °C (d)

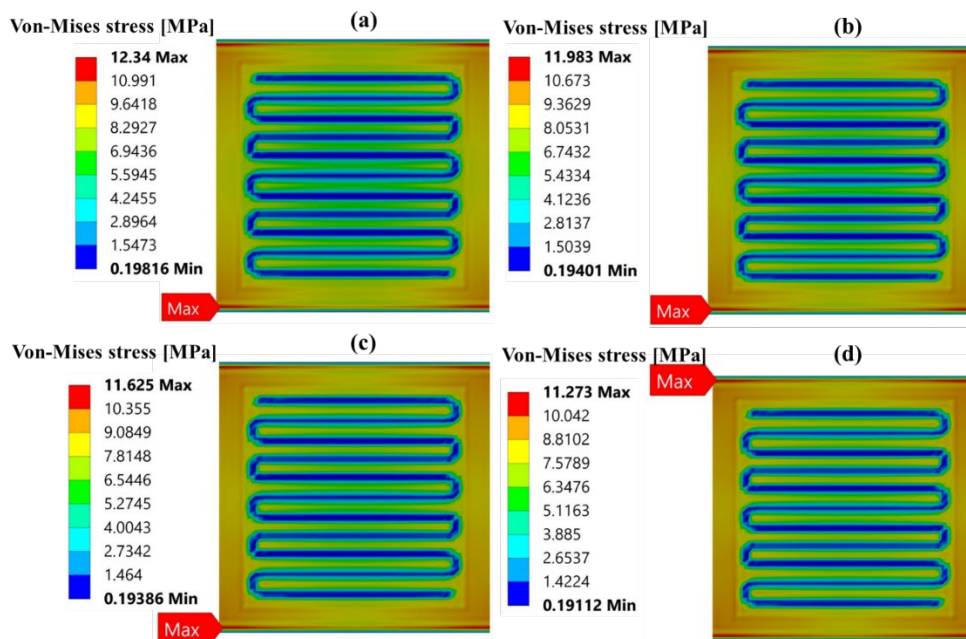


Figure 5. Combined effect of clamping torque and temperature on the von Mises stress distribution in the PEMFC membrane

Figure 4 presents the membrane thermal stress distributions at operating temperatures of 50 °C, 60 °C, 70 °C, and 80 °C, which result from the differential thermal expansion coefficients of the individual cell components. As the operating temperature increases from 50 °C to 80 °C, the maximum thermal stress rises from 1.0059 MPa to 2.0836 MPa. This results in an absolute increase of 1.0777 MPa, indicating that the maximum thermal stress at 80 °C is nearly double that at 50 °C.

The maximum thermal stress obtained in this study agrees with previously reported results. Li et al. [24] numerically investigated the thermal stress behavior of PEM-type membranes under various temperature gradients, reporting thermal stress values ranging from 0.33 MPa to 2 MPa at 313 K. This phenomenon is attributed to the thermal expansion mismatch between the membrane and the adjacent layers, which becomes more pronounced at higher temperatures.

The maximum stresses tend to concentrate near the edges and corners of the membrane, where structural constraints limit thermal expansion. In contrast, the central region of the membrane experiences relatively lower stresses due to a more uniform temperature distribution. These thermal stresses are significant, as they can lead to localized deformation or micro-crack formation during prolonged operation, even without humidity-induced swelling [25]. Figure 5 shows the combined thermo-mechanical stress distribution in the PEMFC membrane resulting from the applied clamping torque of 10 Nm under different operating temperatures. As the operating temperature increased from 50 °C to 80 °C, the thermo-mechanical stresses generated in the membrane gradually decreased, with the maximum stress showing a reduction of approximately 9%. In general, engineering materials experience dimensional changes with increasing temperature due to thermal expansion. Similarly, the fuel cell undergoes outward expansion under thermal effects [26]. According to Hooke's law, an increase in strain directly results in an increase in stress. In the present analysis, the temperature-dependent variation of the elastic modulus was neglected, and the material stiffness was assumed to remain constant. Consequently, the membrane exhibited a certain displacement solely as a result of thermal expansion. When the clamping torque was subsequently applied as a boundary condition, the displacement magnitude was reduced because the mechanical constraint limited the free thermal expansion of the cell components. As a result of this displacement reduction, the von Mises stress values in the membrane also decreased. These findings indicate that mechanical compression not only governs the overall stress state but also counteracts part of the thermally induced stresses, emphasizing the importance of considering both thermal and mechanical loads in the structural design of PEMFCs.

4. Conclusion

In this study, a solid mechanics and steady-state thermal coupled simulation model of a low-temperature PEMFC was developed, and finite element analyses were performed to evaluate the thermo-mechanical stresses induced during cell assembly under a clamping torque of 10 Nm and

various operating temperatures. The thermal stresses induced in the membrane, which is the core component of the PEM fuel cell, were evaluated under different operating temperatures, while the inclusion of a clamping torque in the model enabled the calculation of the resulting thermo-mechanical stresses. Thermal stresses in the membrane increased with rising temperature, reaching a maximum of 2.0836 MPa at 80 °C. The numerical results indicated that increasing the operating temperature from its minimum to maximum gradually decreased the thermo-mechanical stresses within the membrane, with the peak stress diminishing by nearly 9%. These findings emphasize that mechanical compression governs the stress distribution and mitigates thermal effects. This study highlights the need to consider thermal and mechanical loads in the structural design of PEMFCs. Overall, the findings of this study provide valuable insights for the structural optimization of PEM fuel cells, thereby supporting the advancement of sustainable and environmentally friendly energy technologies.

Article Information Form

The Declaration of Conflict of Interest/ Common Interest

No conflict of interest or common interest has been declared by the author.

Artificial Intelligence Statement

No artificial intelligence tools were used while writing this article.

Copyright Statement

The author owns the copyright of their work published in the journal and their work is published under the CC BY-NC 4.0 license.

References

- [1] A. Kumari, et al., "Optimization of air-cooled PEM fuel cell system with battery hybridization and experimental validation on hydrogen powered fuel cell bike," *Renew. Energy*, vol. 250, p. 123340, Jan 2025. doi: 10.1016/j.renene.2025.123340. [Online]. Available: <https://doi.org/10.1016/j.renene.2025.123340>

- [2] Q. Wang, J. Lu, W. Zheng, B. Li, J.P. Zheng, G. Cui, L. Hao, and P. Ming, "Dynamic thermal and mass transport in PEM fuel cells at elevated temperatures and pressures: A 3D model study," *Fuel*, vol. 381, p. 133623, Feb 2025. doi: 10.1016/j.fuel.2024.133623. [Online]. Available: <https://doi.org/10.1016/j.fuel.2024.133623>
- [3] A. Alaswad, A. Baroutaji, H. Achour, J. Carton, A. al Makky, and A. G. Olabi, "Developments in fuel cell technologies in the transport sector," *Int. J. Hydrog. Energy*, vol. 41, no. 37, pp. 16499–16508, Oct 2016. doi: 10.1016/j.ijhydene.2016.03.164. [Online]. Available: <https://doi.org/10.1016/j.ijhydene.2016.03.164>
- [4] R. M. N. Javed, A. A. Othman, M. Tawalbeh, and A. G. Olabi, "Recent developments in graphene and graphene oxide materials for polymer electrolyte membrane fuel cells applications," *Renew. Sustain. Energy Rev.*, vol. 168, p. 112836, Oct 2022. doi: 10.1016/j.rser.2022.112836. [Online]. Available: <https://doi.org/10.1016/j.rser.2022.112836>
- [5] N. A. A. Qasem and G. A. Q. Abdulrahman, "A Recent comprehensive review of fuel cells: history, types, and applications," *Int. J. Energy Res.*, vol. 2024, Art. no. 7271748, 2024. doi: 10.1155/2024/7271748. [Online]. Available: <https://doi.org/10.1155/2024/7271748>
- [6] S. Zhang, X. Yuan, H. Wang, W. Mérida, H. Zhu, J. Shen, S. Wu, and J. Zhang, "A review of accelerated stress tests of MEA durability in PEM fuel cells," *Int. J. Hydrog. Energy*, vol. 34, no. 1, pp. 388–404, Jan 2009. doi: 10.1016/j.ijhydene.2008.10.012. [Online]. Available: <https://doi.org/10.1016/j.ijhydene.2008.10.012>
- [7] E. Wallnöfer-Ogris, F. Poimer, R. Köll, M. G. Macherhammer, and A. Trattner, "Main degradation mechanisms of polymer electrolyte membrane fuel cell stacks – Mechanisms, influencing factors, consequences, and mitigation strategies," *Int. J. Hydrog. Energy*, vol. 50, pp. 1159–1182, Jan 2024. doi: 10.1016/j.ijhydene.2023.06.215. [Online]. Available: <https://doi.org/10.1016/j.ijhydene.2023.06.215>
- [8] R. B. Ferreira, D. S. Falcão, and A. M. F. R. Pinto, "Simulation of membrane chemical degradation in a proton exchange membrane fuel cell by computational fluid dynamics," *Int. J. Hydrog. Energy*, vol. 46, no. 1, pp. 1106–1120, Jan 2021. doi: 10.1016/j.ijhydene.2020.09.179. [Online]. Available: <https://doi.org/10.1016/j.ijhydene.2020.09.179>
- [9] W. Jiang, K. Zhang, X. Huang, Z. Cai, J. Zheng, Y. Kai, B. Zheng, and K. Song, "Influence of clamping pressure on contact pressure uniformity and electrical output performance of proton exchange membrane fuel cell," *Appl. Energy*, vol. 353, p. 122021, Jan 2024. doi: 10.1016/j.apenergy.2023.122021. [Online]. Available: <https://doi.org/10.1016/j.apenergy.2023.122021>
- [10] S. N. Ozdemir and E. Kurt, "A finite element modeling of PEMFC stack assembly under a novel hydraulic clamping mechanism," *Environ. Prog. Sustain. Energy*, vol. 44, no. 1, p. e14649, Jan 2025. doi: 10.1002/ep.14649. [Online]. Available: <https://doi.org/10.1002/ep.14649>
- [11] B. Yilgin, C. Celik, and F. G. Boyaci San, "Clamping effects on the performance of proton exchange membrane fuel cell," *Int. J. Hydrog. Energy*, vol. 141, pp. 888–895, Jan 2025. doi: 10.1016/j.ijhydene.2024.12.015. [Online]. Available: <https://doi.org/10.1016/j.ijhydene.2024.12.015>

- [12] G. Jing, C. Hu, Y. Qin, X. Sun, and T. Ma, "Complex mechanisms of PEMFC performance variations influenced by both structural deformation and contact resistance under the clamping force," *Int. J. Hydrog. Energy*, vol. 58, pp. 137–148, Mar 2024. doi: 10.1016/j.ijhydene.2024.01.164. [Online]. Available: <https://doi.org/10.1016/j.ijhydene.2024.01.164>
- [13] K. Oh, P. Chippar, and H. Ju, "Numerical study of thermal stresses in high-temperature proton exchange membrane fuel cell (HT-PEMFC)," *Int. J. Hydrog. Energy*, vol. 39, no. 6, pp. 2785–2794, Feb 2014. doi: 10.1016/j.ijhydene.2013.01.201. [Online]. Available: <https://doi.org/10.1016/j.ijhydene.2013.01.201>
- [14] A. Bates, S. Mukherjee, S. Hwang, S. C. Lee, O. Kwon, G. H. Choi, and S. Park, "Simulation and experimental analysis of the clamping pressure distribution in a PEM fuel cell stack," *Int. J. Hydrog. Energy*, vol. 38, no. 15, pp. 6481–6493, May 2013. doi: 10.1016/j.ijhydene.2013.03.049. [Online]. Available: <https://doi.org/10.1016/j.ijhydene.2013.03.049>
- [15] M. A. R. Sadiq Al-Baghdadi, "A CFD study of hygro-thermal stresses distribution in PEM fuel cell during regular cell operation," *Renew. Energy*, vol. 34, no. 3, pp. 674–682, Mar 2009. doi: 10.1016/j.renene.2008.05.023. [Online]. Available: <https://doi.org/10.1016/j.renene.2008.05.023>
- [16] X. Sun, P. Wen, Q. Zhang, G. Jing, and T. Ma, "Numerical investigation of structural deformation of gas diffusion layer and contact resistance under assembly force effect on proton exchange membrane fuel cell performance," *J. Power Sources*, vol. 630, p. 236120, Jan 2025. doi: 10.1016/j.jpowsour.2024.236120. [Online]. Available: <https://doi.org/10.1016/j.jpowsour.2024.236120>
- [17] P. Chippar, K. Oh, D. Kim, T. W. Hong, W. Kim, and H. Ju, "Coupled mechanical stress and multi-dimensional CFD analysis for high temperature proton exchange membrane fuel cells (HT-PEMFCs)," *Int. J. Hydrog. Energy*, vol. 38, no. 18, pp. 7715–7724, June 2013. doi: 10.1016/j.ijhydene.2012.07.122. [Online]. Available: <https://doi.org/10.1016/j.ijhydene.2012.07.122>
- [18] J. Zhang, Y. Hu, C. Han, and H. Zhang, "Stress response and contact behavior of PEMFC during the assembly and working condition," *Int. J. Hydrog. Energy*, vol. 46, no. 59, pp. 30467–30478, Aug 2021. doi: 10.1016/j.ijhydene.2021.06.200. [Online]. Available: <https://doi.org/10.1016/j.ijhydene.2021.06.200>
- [19] M. A. R. S. Al-Baghdadi, "Three-dimensional solid mechanics-CFD modeling of a PEM fuel cell stack," *Int. J. Energy Environ.*, vol. 9, no. 1, pp. 1-26, 2018. [Online]. Available: <http://www.ijee.ieefoundation.org/>
- [20] G. Varghese, K. P. Babu, T. V. Joseph, and P. Chippar, "A numerical investigation on thermal gradients and stresses in high temperature pem fuel cell during start-up," *Int. J. Heat Mass Transf.*, vol. 175, p. 121365, Aug 2021. doi: 10.1016/j.ijheatmasstransfer.2021.121365. [Online]. Available: <https://doi.org/10.1016/j.ijheatmasstransfer.2021.121365>
- [21] Z. Zhan, H. Zhao, P. C. Sui, P. Jiang, M. Pan, and N. Djilali, "Numerical analysis of ice-induced stresses in the membrane electrode assembly of a PEM fuel cell under sub-freezing operating conditions," *Int. J. Hydrog. Energy*, vol. 43, no. 9, pp. 4563–4582, Mar 2018. doi:

- 10.1016/j.ijhydene.2018.01.064. [Online]. Available: <https://doi.org/10.1016/j.ijhydene.2018.01.064>
- [22] S. N. Özdemir, İ. Taymaz, and E. Kurt, "Finite element method modeling and optimization of the mechanical behavior of a low-temperature PEM fuel cell," *Pamukkale Univ. J. Eng. Sci.*, vol. 30, no. 6, pp. 715–728, 2024. doi: 10.5505/pajes.2023.45773. [Online]. Available: <https://doi.org/10.5505/pajes.2023.45773>
- [23] J. Shen, C. Zhang, L. Li, S. Liu, H. Liu, B. Chen, and C. Du, "Numerical study and prediction of water transport through a PEM fuel cell based on genetic algorithm," *Energy*, vol. 308, p. 132851, Oct 2024. doi: 10.1016/j.energy.2024.132851. [Online]. Available: <https://doi.org/10.1016/j.energy.2024.132851>
- [24] L. Shian, C. Peng, Q. Shen, Y. Cheng, C. Wang, and G. Yang, "Numerical study on thermal stress of high temperature proton exchange membrane fuel cells during start-up process," *Membranes*, vol. 13, no. 2, p. 215, Feb 2023. doi: 10.3390/membranes13020215. [Online]. Available: <https://doi.org/10.3390/membranes13020215>
- [25] S. Shi, J. Li, H. Li, Y. Yao, H. Dai, Y. Fu, Q. Lin, and X. Chen, "Temperature-dependent fatigue crack growth mechanisms of fuel cell membranes," *Int. J. Fatigue*, vol. 154, p. 106554, Jan 2022. doi: 10.1016/j.ijfatigue.2021.106554. [Online]. Available: <https://doi.org/10.1016/j.ijfatigue.2021.106554>
- [26] N. Shah, X. Xu, J. Love, H. Wang, Z. Zhu, and L. Ge, "Mitigating thermal expansion effects in solid oxide fuel cell cathodes: A critical review," *J. Power Sources*, vol. 599, p. 234211, Apr 2024. doi: 10.1016/j.jpowsour.2024.234211. [Online]. Available: <https://doi.org/10.1016/j.jpowsour.2024.234211>